Covalent or Non-Covalent? A Mechanistic Insight into the Enantioselective Brønsted Acid Catalyzed Dearomatization of Indoles with Allenamides

Covalent or Non-Covalent? A Mechanistic Insight into the Enantioselective Brønsted Acid Catalyzed Dearomatization of Indoles with Allenamides

Pietro Giacinto,[a] Andrea Bottoni,[a] Andrea Garelli,[a] Gian Pietro Miscione,*[b] and Marco Bandini*[a]

The reaction mechanism of the enantioselective Brønsted acid catalyzed dearomatization of C(2),C(3)-disubstituted indoles with allenamides is investigated by means of density functional theory (DFT) calculations and ESI-MS analysis. The first step of the process (rate-determining step) is the formation of a covalent adduct between allenamide and the chiral organo-promoter. The resulting chiral α-amino allylic phosphate undergoes dearomative condensation with indoles. In the first step, the indole moiety remains bonded to the catalyst through strong hydrogen contacts. It can take on two different orientations that make the *Re* or *Si* prochiral face available to the subsequent electrophilic attack of allenamide. The attack on the indole faces originates two reaction paths leading to different stereoisomeric products, which differ in the configuration of the new stereocenter at the C3-indole position.

Introduction

The phosphoric Brønsted acid (BA) catalyzed synthesis of added value building blocks is in continuous expansion within the asymmetric synthesis context.[1] Current trends deal with the development of new and always more efficient chiral promoters[2] as well as new organic transformations.[1]

This approach is commonly described as "asymmetric counteranion-directed catalysis" (ACDC).[3] It is based on the instauration of non-covalent ionic contacts between the proto-activated substrate (generally an electrophilic species) and the resulting chiral anion. The term "weak interaction catalysis" is also used (see Figure 1 a). Bifunctional catalytic activation modes, played by the chiral entity, are frequently invoked through simultaneous interactions with both reaction partners. Furthermore, in a few cases, a covalent catalysis involving the temporary *addition* of the chiral catalyst to the electrophilic partner has been proposed to get a better understanding of the excellent stereochemical translations experimentally observed (Figure 1 b).

Important examples for the latter mechanistic hypothesis rely on the intramolecular hydroamination of dienes assisted by dithiophosphoric acids **BA1** (Toste and co-workers, Scheme 1 a)[4a] and the aminative cyclization of unsaturated acetals promoted by classic chiral O-based phosphoric acid **BA2** (Zimmerman, Nagorny and colleagues, Scheme 1 b).[4b] In the former case, the presence of "covalent" dithiophosphate intermediates **A** was proved by mass spectrometry (TOF-MS) and specific control experiments. In the latter case, a computational investigation was carried out to demonstrate the reliability of the "covalent" intermediate (**B**) envisaged in the hypothesized mechanism.

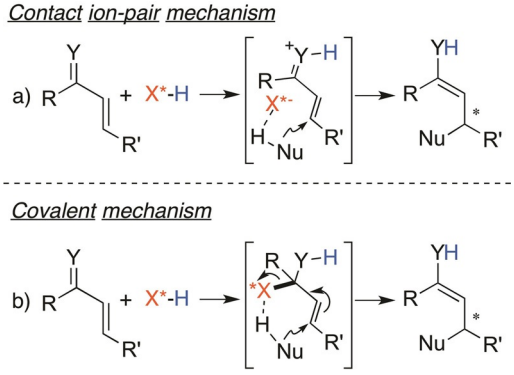

Figure 1. Pictorial representation of classic "non-covalent" (a) and unconventional "covalent" (b) activation modes of strong Brønsted acid catalysis. The case of the nucleophilic conjugate addition to activated π-systems is depicted (X*-H: chiral BA).

Within this scenario and as a part of our ongoing research project concerning both metal-based and metal-free manipulation of indole compounds,[5] we recently addressed the C3-selective dearomatization of 2,3-disubstituted indoles (racemic variant) with allenamides (**2**)[6] in the presence of phosphite gold(I)–TFA complexes. In particular, we examined the role of the TFA counterion on the regiochemistry of the process.[7] Interestingly, the search for an enantioselective variant based on

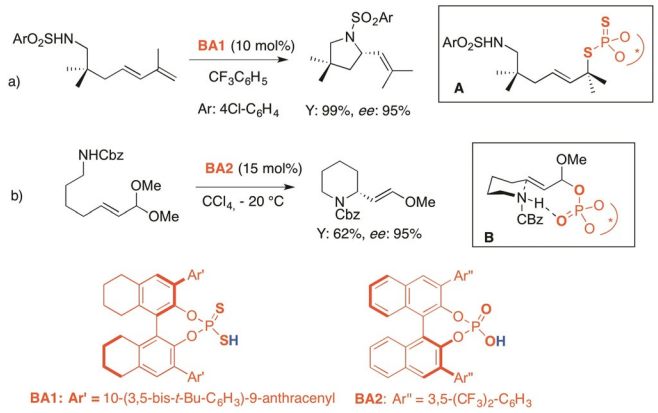

Scheme 1. a) Seminal works invoking covalent electrophilic activations in enantioselective BA catalysis.

asymmetric gold-centered catalysis provided no synthetically useful stereochemical outcomes.[8]

Being aware of the well-known isolobal analogy[9] that frequently interconnects [Au^{I}] cations and the proton, we envisioned to overcome this impasse by means of chiral Brønsted acid catalysis.[10,11] An extensive optimization step of the reaction conditions was carried out, leading to BINOL-based phosphoric acid (*S*)-C_8TCyP[12] **BA3** (1–10 mol%) as the optimal promoter along with anhydrous benzene as the reaction medium. Under these conditions, a number of diversely functionalized indoline cores **3**, featuring all-carbon quaternary stereogenic centers at the C3-position, were isolated in high yields and enantiomeric excesses up to 94% (Scheme 2).

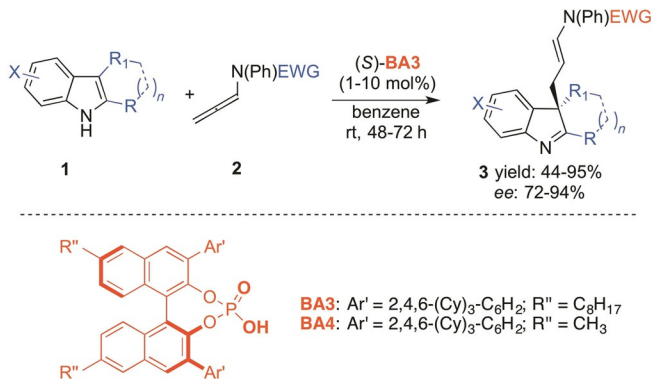

Scheme 2. General scheme highlighting optimal reaction conditions for the metal-free dearomatization of indoles.

Additionally, the simultaneous combination of the stereoselective dearomative partners and the metal-free reductant Hantzsch ester (HE)[13] enabled the isolation with very high stereoselectivity of the corresponding indoline cores featuring two adjacent stereogenic centers.

The recorded chemical reactivity was ascribed to the initial protonation of the central carbon atom of the allenyl unit (namely Cβ in Figure 2)[14] by the chiral phosphoric acid (BA-H) with consequent generation of the electrophilic adduct **A**. Subsequent regioselective trapping of **A** by C(3)-substituted

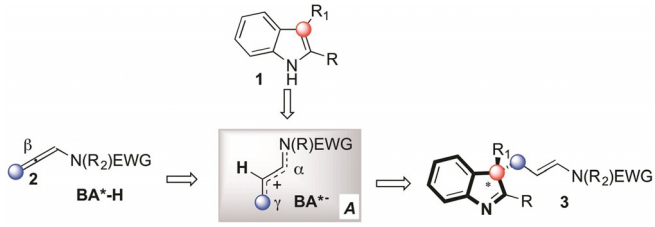

Figure 2. General scheme accounting for the electrophilic activation of **2** and subsequent nucleophilic trapping by the indole.

indoles led to the indoline core **3** through a formal allylative[15] dearomatizing protocol.[16]

Besides the intrinsic efficiency of the above-discussed synthetic approach, two main questions concerning the mechanism of the process are still open. In particular:

(i) What is the real activation mechanism of the substrate, that is, is it covalent or non-covalent catalysis?

(ii) How can we explain the overall stereochemical outcome of this synthetic methodology, given that the (*S*)-**3** compound was obtained as the major stereoisomer?

In this paper, we discuss the results of a combined computational/experimental investigation that we carried out to elucidate the above mechanistic aspects. We used a density functional theory (DFT) approach to explore the reaction surface. The model system was formed of two substrates, that is, 2,3-dimethyl-indole (**1a** with R=R^1=Me, X=H, Scheme 2) and *N*-phenyl-*N*-sulfonylallenamide (**2a** with electron-withdrawing groups (EWG)=Ts, R^2=Ph), and the chiral catalyst (*S*)-C_8-TCyP **BA4** (Scheme 2) where the alkyl chains C_8H_{17} on the BINOL skeleton of the chiral BA were replaced with methyl groups. Furthermore, an ionic trap mass spectrometry analysis was carried out to provide experimental support for the hypothesized covalent mechanism.

Results and Discussion

Computation of the potential reaction surface

The DFT investigation of the reaction potential surface demonstrated the existence of two-step reaction pathways. These lead to the two possible stereoisomers differing in the configuration of the new stereocenter at the C(3)-position. A schematic representation of the corresponding reaction profiles is given in Figure 3.

At the beginning of the process, the catalyst structure allows a simultaneous interaction of the two reactants (i.e., indole and allenamide) with the catalytic center. In the resulting initial molecular aggregate (or initial complex) the indole planar system and allenamide are stacked and the catalyst cyclohexyl groups surround them. The two molecules interact with the phosphate group through two hydrogen bonds involving the phosphate oxygen atoms (O1 and O2), the indole N1H2 bond, and the N2 and Cα atoms of the allenamide moiety. The role of the catalyst in this case recalls the "proximity effect" invoked to rationalize enzymatic reactions, where the catalytic action of enzymes is partly due to their capacity of

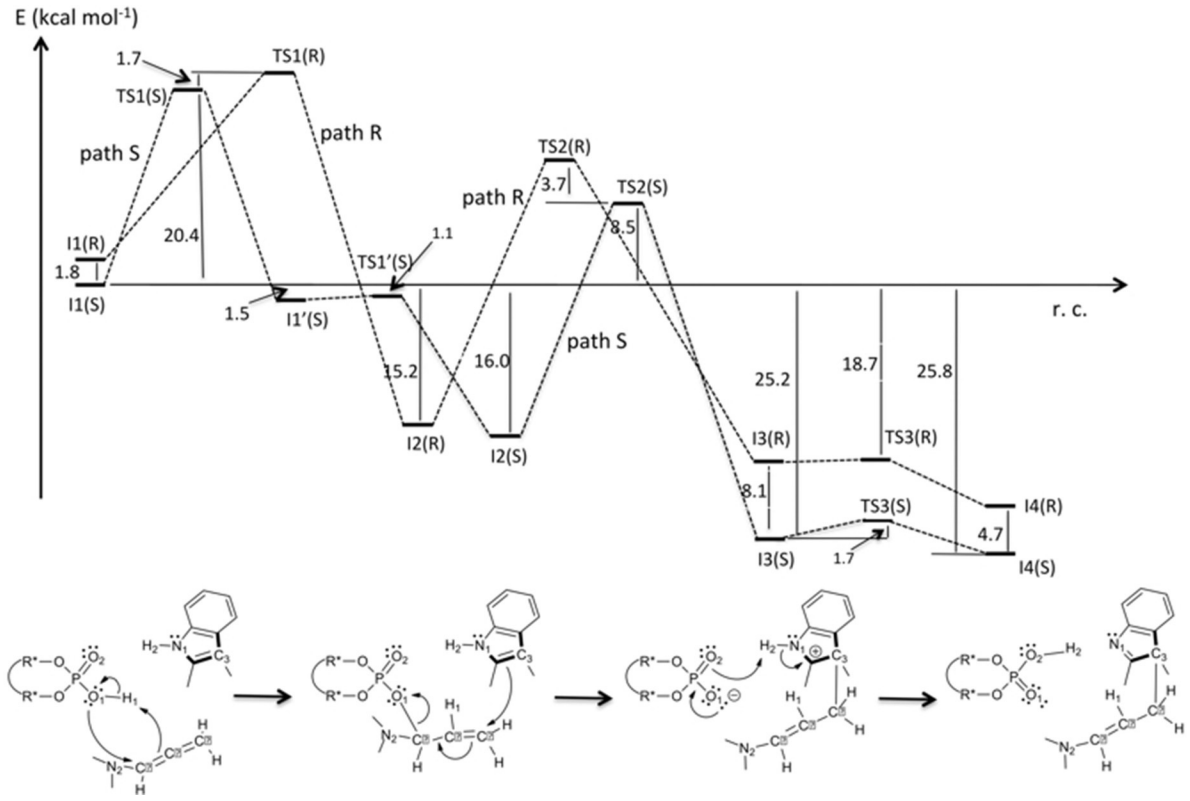

Figure 3. A schematic representation of the reaction profiles computed for path S and path R leading to the stereoisomeric products **I4(*S*)** and **I4(*R*)**, respectively. At the bottom of the figure is a schematic representation of the reaction.

bringing the reactants into close proximity. Similarly, here the effect of the catalyst can result in part from its capacity of gathering together the two reactant molecules. Two possible structural arrangements of the complex involving the catalyst and substrates make the *Re* or *Si* prochiral faces of the indole (the nucleophile) available to the electrophilic attack of the allenamide. The corresponding initial complexes are denoted as **I1(*R*)** and **I1(*S*)**, respectively.

Figure 4 shows a three-dimensional representation of **I1(*S*)**: the stacking of the indole planar system and allenamide and the "cage" effect played by the catalyst are evident. The attacks on the two faces of the indole originate the two different reaction paths (denoted as path R and path S) of Figure 3. Along these two reaction channels, the reactants are forced to maintain the initial relative position resulting in two possible isomeric forms (**I4(*R*)** and **I4(*S*)**) of the final product.

More schematic representations of **I1(*S*)** and **I1(*R*)** are reported in Figure 5 and Figure S2 in the Supporting Information. As the different relative orientations of the cyclohexyl groups of the catalyst can originate several different conformational isomers for these two intermediates, we carefully investigated the corresponding conformational space. We located other possible structures for **I1(*R*)** and **I1(*S*)**, but all at higher energy. The Cartesian coordinates for these conformational isomers and the corresponding energy values are reported in the Supporting Information.

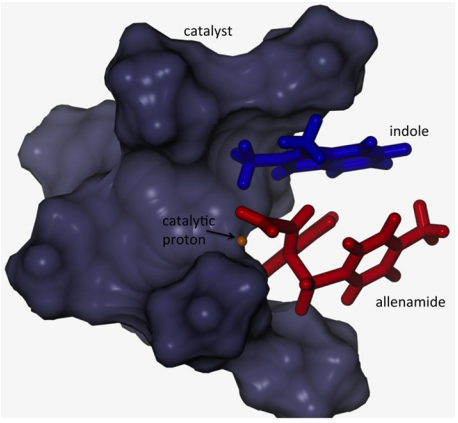

Figure 4. A three-dimensional representation of the starting molecular aggregate **I1(*S*)** showing the stacked arrangement of indole and allenamide.

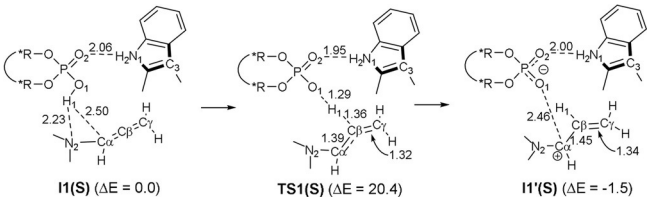

Figure 5. A schematic representation of the structures of **I1(*S*)**, **TS1(*S*)**, **I1'(*S*)**. Bond lengths are in Angstroms. Energy values are in kcal mol-1 and refer to initial complex **I1(*S*)**.

The complex **I1(*S*)**, with indole exposing the *Si* face to allenamide, is 1.8 kcal mol^{-1} more stable than **I1(*R*)** (indole exposing the *Re* face). The factors determining the different energy of **I1(*R*)** and **I1(*S*)** are the hydrogen interactions between **BA4** and the substrates and the smaller steric clashes between the catalyst cyclohexyl groups and indole methyl groups, with the smallest distances between these two groups being 2.34 Å and 2.40 Å in **I1(*R*)** and 2.52 Å and 2.66 in in **I1(*S*)**. Although the hydrogen bond O2···H2N1 is almost identical in the two complexes (O2···H2 distance is 2.06 Å in **I1(*S*)** and 2.07 Å in **I1(*R*)**), a much more significant change was observed for the N2···H1O1 contact, which involves the electron-rich allenamide system. In this case, the N2···H1 distance varies from 2.23 Å in **I1(*S*)** to 2.58 Å in **I1(*R*)**, suggesting a more important stabilizing effect in the former case. An opposite trend, although less pronounced and, thus less important, was found for the Cα···H1O1 interaction, the Cα···H1 distance being 2.50 and 2.29 Å in **I1(*S*)** and **I1(*R*)**, respectively.

As the molecular transformations occurring along the two reaction pathways are very similar, we discuss in detail the mechanism detected along the more stable path S (attack on the indole *Si* face). The structures corresponding to the various critical points located along path S are schematically represented in Figure 5 (**I1(*S*)**, **TS1(*S*)**, **I1′(*S*)**), Figure 6 (**TS1′(*S*)**, **I2(*S*)**, **TS2(*S*)**), and Figure 7 (**I3(*S*)**, **TS3(*S*)**, **I4(*S*)**).

In the first step, the transfer of the phosphate acidic catalytic proton, H1, to carbon Cβ activates the allenamide molecule. In the corresponding transition state, **TS1(*S*)**, H1 is approximately half way between O1 and Cβ (O1···H1 = 1.29 Å and H1···Cβ = 1.36 Å), whereas the O1···Cα distance is still rather large (3.13 Å). As the electron pair of the Cα–Cβ π bond is used to bind H1, the proton transfer has the effect of making Cα much more positive (and hence much more electrophilic): the Cα net charge (electrostatic potential (ESP) charge) varies from −0.23 in **I1(*S*)** to +0.30 in **TS1(*S*)**. The energy barrier for **TS1(*S*)** is rather high (20.4 kcal mol^{-1}), in agreement with activation barriers computed elsewhere for "non-assisted" proton transfer.[17] In the resulting intermediate **I1′(*S*)**, O1 is much closer to Cα (the O1···Cα distance is 2.46 Å), a more appropriate arrangement for the subsequent nucleophilic attack on the positive carbon. H1 is definitely bonded to Cβ, which determines a further increase of the positive charge on the allenamide Cα (+0.61) and a simultaneous increase of the negative charge on the phosphate moiety (as indicated by the shortening of the O2–H2 distance, which is 2.00 Å in **I1′(*S*)**). This negative charge is delocalized over O1 and O2. In agreement with the charge delocalization, the P–O1 and P–O2 bond lengths are 1.49 Å and 1.50 Å, respectively.

Despite the appearance of two opposite charges, **I1′(*S*)** is slightly more stable (1.5 kcal mol^{-1}) than **I1(*S*)**: reasonably, this is due to the charge delocalization on allenamide (positive charge) and phosphate (negative charge). A very small activation barrier (only 0.4 kcal mol^{-1}) must be overcome to complete the nucleophilic attack and form the O1–Cα bond (1.47 Å), that is, the **I2(*S*)** intermediate where allenamide is covalently bonded to the catalyst. The transition state, **TS1′(*S*)** (1.1 kcal mol^{-1} below the initial complex), can be reasonably considered a computational shortcoming with no real experimental meaning. It simply suggests a very asynchronous, concerted process where the proton transfer and nucleophilic attack occur in two different phases of a unique kinetic step. A comparison between **I1(*S*)** and **I2(*S*)** shows that a σ bond has replaced a π bond, which results in an overall energy stabilization of 16.0 kcal mol^{-1}.

In this initial reaction stage (**I1(*S*)**→**I2(*S*)**), the indole ring behaves as a "spectator" without being involved in new bond formation. It remains glued to the catalyst by means of the strong H2···O2 hydrogen bond: the H2···O2 distance is 2.14 Å in **I2(*S*)** after the formation of the O1–Cα bond. The existence of this covalent intermediate allows us to confirm an overall S_N2'-type mechanism and consequently discards the hypothetical indole Michael-type addition on a protonated α,β-unsaturated iminium intermediate. As a matter of fact, the latter reaction machinery was not located in spite of extensive search.

Interestingly, the transfer of the H1 proton and the formation of the covalent adduct also causes a significant increase of the electrophilic character at the Cγ carbon atom in **I2(*S*)** (its net ESP charge becomes −0.38, whereas it was −0.59 in **I1(*S*)**). This makes the nucleophilic attack of the indole C(3) atom on the Cγ-carbon atom of allenamide easier to occur in the next step of the process. The formation of the new σ bond Cγ–C3 requires the overcoming of an intrinsic energy barrier of 24.5 kcal mol^{-1}. However, as the corresponding transition state **TS2(*S*)** is 8.5 kcal mol^{-1} above the starting complex, **TS1(*S*)** remains the rate-determining step of the process.

TS2(*S*) leads to the formation of a new stereogenic center at C3 (the Cγ–C3 distance is 2.42 Å in **TS2(*S*)**) with the simultaneous dearomatization of the indole system. The transfer of electron density from the indole ring to the Cγ carbon atom causes a change in the nature of the Cγ–Cβ and Cβ–Cα

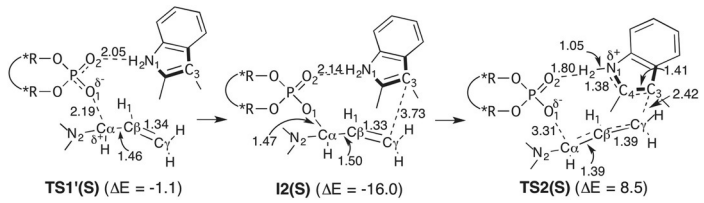

Figure 6. A schematic representation of the structure of **TS1′(*S*)**, **I2(*S*)**, **TS2(*S*)**. Bond lengths are in Angstroms. Energy values are in kcal mol-1 and refer to initial complex **I1(*S*)**.

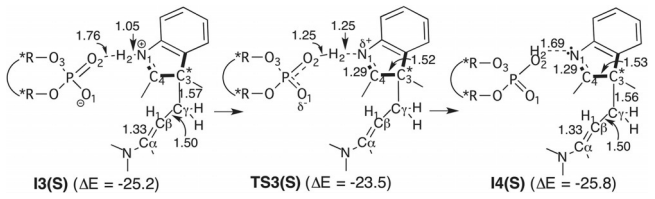

Figure 7. A schematic representation of the structure of **I3(*S*)**, **TS3(*S*)**, **IS4(*S*)**. Bond lengths are in Angstroms. Energy values are in kcal mol-1 and refer to initial complex **I1(*S*)**.

bonds: whereas the former converts into a single bond, the latter changes to a double bond (the corresponding bond lengths are both 1.39 Å). Consequently, the Cα–O1 bond breaks (the Cα–O1 distance becomes 3.31 Å in **TS2(*S*)**) and the catalyst moves away from the allenamide.

Another consequence of the electronic rearrangement is the increase of the negative charge on the phosphate fragment, as evident from the remarkable strengthening of the H2···O2 hydrogen bond (H2···O2 = 1.80 Å in **TS2(*S*)**). However, in spite of the strength of this hydrogen contact, the H2 proton remains strongly bonded to N1, the H2–N1 bond length being 1.05 Å. Furthermore, the electron reorganization occurring after the nucleophilic attack of C3 on allenamide, determines the increase of the N1=C4 double bond character (1.38 Å in **TS2(*S*)**). Simultaneously, the C4=C3 double bond changes into a single bond, its length being 1.41 Å in **TS2(*S*)** and 1.38 Å in **I2(*S*)**.

In spite of the indole dearomatization, the formation of the new single C–C bond (Cγ–C3 = 1.57 Å) leads to a rather stable intermediate, **I3(*S*)**, which lies 25.2 kcal mol^{-1} below the initial complex. The dearomatization process does not affect significantly the stability of **I3(*S*)** because it involves the pyrrolic ring and not the fused benzene ring where the aromatic stabilization is much more important. Because of the Cγ–C3 bond formation in **I3(*S*)**, the prochiral sp^2-hybridized C(3) carbon atom has changed to a sp^3 stereocenter with *S* configuration. As mentioned previously, a final proton transfer, in which H2 moves definitely from N1 to O2, is needed to deliver the final products and regenerate the catalyst. In **I3(*S*)**, in spite of the very short H2···O2 distance (only 1.76 Å), H2 is still tightly bonded to the indole system (H2···N1 distance = 1.05 Å), which has a formal positive charge stabilized by ring delocalization. A very low barrier (only 1.7 kcal mol^{-1}) must be surmounted (transition state **TS3(*S*)**) to obtain the final product **I4(*S*)** and restore the catalyst. The fact that H2 in **I3(*S*)** is almost shared between O2 and N1 (and the simultaneous formation of the π P–O1 bond), explains the low activation energy. The final product, **I4(*S*)**, is slightly more stable than **I3(*S*)**. This is consistent with the very similar electronic structure of **I3(*S*)** and **I4(*S*)**, where the H2 proton is still very close to N1, the N1···H2 distance being 1.69 Å.

The mechanism detected along path R (where the attack on allenamide involves the indole prochiral *Re* face) is very similar to that previously discussed. The only difference is the lack of the **I1(*R*)′** intermediate, as found along path S. This does not change the general features of the **I1(*R*)**→**I2(*R*)** transformation (representing the activation phase of the allenamide), that is, a very asynchronous concerted process (as outlined for the path S mechanism) where the possible presence of the **I1′** intermediate must be considered a computational artifact that does not affect the general mechanistic scenario. As all critical points located along path R are very similar to those we could find for the path S mechanism, we do not describe them in detail. A schematic representation of these structures is given in Figures S2–S3 (in the Supporting Information).

Importantly, all critical points on path S are more stable than the corresponding structures on path R. We have previously shown for the starting complexes **I1(*R*)** and **I1(*S*)** that the different stability is determined by a better fitting of reactant species in the chiral catalyst pocket. This corresponds to less steric encumbrance and stronger and more stabilizing non-covalent interactions (hydrogen bonds). For similar reasons, **TS1(*S*)** (which represents the rate-determining step of the reaction) is more stable than **TS1(*R*)** and the energy gap favoring path S, which increases in the second part of the process (**I2** → **I4** transformation). In particular, **TS2(*S*)** is 3.7 kcal mol^{-1} more stable than **TS2(*R*)** and the energy gap becomes 4.7 kcal mol^{-1} when we compare the **I4(*S*)** and **I4(*R*)** products.

The energy difference between **TS2(*S*)** and **TS2(*R*)** is reasonably due to the different arrangement of the indole group and, consequently, a stronger indole–catalyst hydrogen bond in **TS2(*S*)** (O2···H2 = 1.80 Å) than in **TS2(*R*)** (O2···H2 = 1.89 Å). Other factors determining the lower energy of **TS2(*S*)** are closer non-bonding contacts between the cyclohexyl C–H bonds and the indole π-system in a T-shaped arrangement, the distance between the benzene centroid and the closest of these C–H bonds being 2.47 Å in **TS2(*S*)** and 3.22 Å in **TS2(*R*)**.

The reaction profiles in Figure 3 can explain the experimental results showing 92% *ee* for the *S* enantiomer. Let us consider the rate-determining step of the reaction (i.e., **I1**→**I2**). The diagram of Figure 3 shows that **I1(*S*)** is more stable than **I1(*R*)** and, consequently, the population of **I1(*S*)** is higher. Furthermore, the activation energy of the reaction **I1(*S*)**→**I2(*S*)** is comparable to that of **I1(*R*)**→**I2(*R*)** (20.4 and 20.3 kcal mol^{-1}, respectively). As **I1(*S*)** and **I1(*R*)** react at almost the same rate, the equilibrium of the reactants remains untouched. Accordingly, it is the equilibrium distribution of the two reactants **I1(*S*)** and **I1(*R*)** that determines the product ratio.

To check the accuracy of our results, we carried out single-point computations on all critical points by using the more accurate 6–31 + G* basis set on all atoms in the presence of solvent effects (PCM computations). The computed energies are collected in Table 1.

The new energy values do not change the mechanistic scenario. Importantly, the **I1(*S*)**→**I2(*S*)** (and **I1(*R*)**→**I2(*R*)**) remains the rate-determining step of the process and **I1(*S*)** is more

Table 1. Energy values relative to **I1(*S*)** (kcal mol^{-1}) obtained with the LDBS approach (3–21G*/6-31G*/LANLDZ basis sets) and with single-point computations with the 6–31 + G* basis on all atoms. In all cases, the solvent effects were taken into account with the PCM approach.

	Path R			Path S	
	3–21G*/6–31G*/	6–31 + G*		3–21G*/6–31G*/	6–31 + G*
I1(*R*)	1.8	[4.1]	**I1(*S*)**	0.00	[0.0]
TS1(*R*)	22.1	[24.5]	**TS1(*S*)**	20.4	[19.9]
non-existing			**I1′(*S*)**	−1.5	[+2.0]
non-existing			**TS1′(*S*)**	−1.1	[3.0]
I2(*R*)	−15.1	[−10.7]	**I2(*S*)**	−16.0	[−10.2]
TS2(*R*)	12.2	[11.8]	**TS2(*S*)**	8.5	[11.8]
I3(*R*)	−17.1	[−15.2]	**I3(*S*)**	−25.2	[−21.4]
TS3(*R*)	−17.0	[−15.2]	**TS3(*S*)**	−23.5	[−19.0]
I4(*R*)	−21.1	[−19.1]	**I4(S)**	−25.8	[−21.9]

stable than **I1(*R*)** by 4.1 kcal mol^{-1}. As **TS1(*R*)** is higher than **TS1(*S*)** by 4.6 kcal mol^{-1}, the two activation energies are still very close and we can conclude again that the relative population of **I1(*S*)** and **I1(*R*)** dictates the product ratio. **I1(*R*)** and **I1(*S*)** are still the lowest energy conformational isomers corresponding to the attack on the *Re* or *Si* indole prochiral faces (to check this point 6–31 + G* single-point computations were carried on the other possible conformational isomers; energy values are reported in the Supporting Information). Again, all critical points on path S are more stable than the corresponding structures on path R. In particular, the reaction products **I3(*S*)** and **I4(*S*)** remain significantly more stable than **I3(*S*)** and **I4(*S*)**, the energy difference being 6.2 and 2.8 kcal mol^{-1}, respectively. The only exception concerns **TS2(*R*)** and **TS2(*S*)** that become degenerate, which, however, does not affect the mechanistic scheme.

Ionic trap mass spectrometry analysis

As the activation mode exerted by the chiral proton-based catalyst on the reaction partners implies the formation of 1:1 covalent adducts between allenamide and the catalyst, we tried to account experimentally for the existence of this species by ionic trap mass spectrometry.

The injection of a preformed mixture of the TRIP and allenamide **2a** in CH_2Cl_2 resulted in several diagnostics testifying to the formation of a 1:1 aggregate between the organocatalyst and the allenyl compound (Figure 8). In particular, the signal at $m/z = 1061.025$ was ascribed to the [TRIP + **2a** + Na^+] adduct, whereas the signal at $m/z = 1078.761$ could be rationalized in terms of a [TRIP + **2a** + K^+] aggregate. It is worth mentioning that the free phosphoric acid and unchanged allenamide were also detected, proving evidence for the not complete condensation among them (see also Figure S1 in the Supporting Information). The experimental detection of a 1:1 adduct between allenamide and the catalyst enforces the mechanistic hypothesis that stems from our computations. It is reasonable to believe that at the beginning of the reaction, allenamide forms an adduct with the catalyst through a proton transfer and the formation a covalent bond, without direct involvement of the indole moiety. After formation of the covalent species, the indole can act as a nucleophile, affording the final product.

Conclusions

We carried out a computational investigation on the reaction mechanism of the enantioselective dearomatization of C(2),C(3)-disubstituted indoles with allenamides catalyzed by a

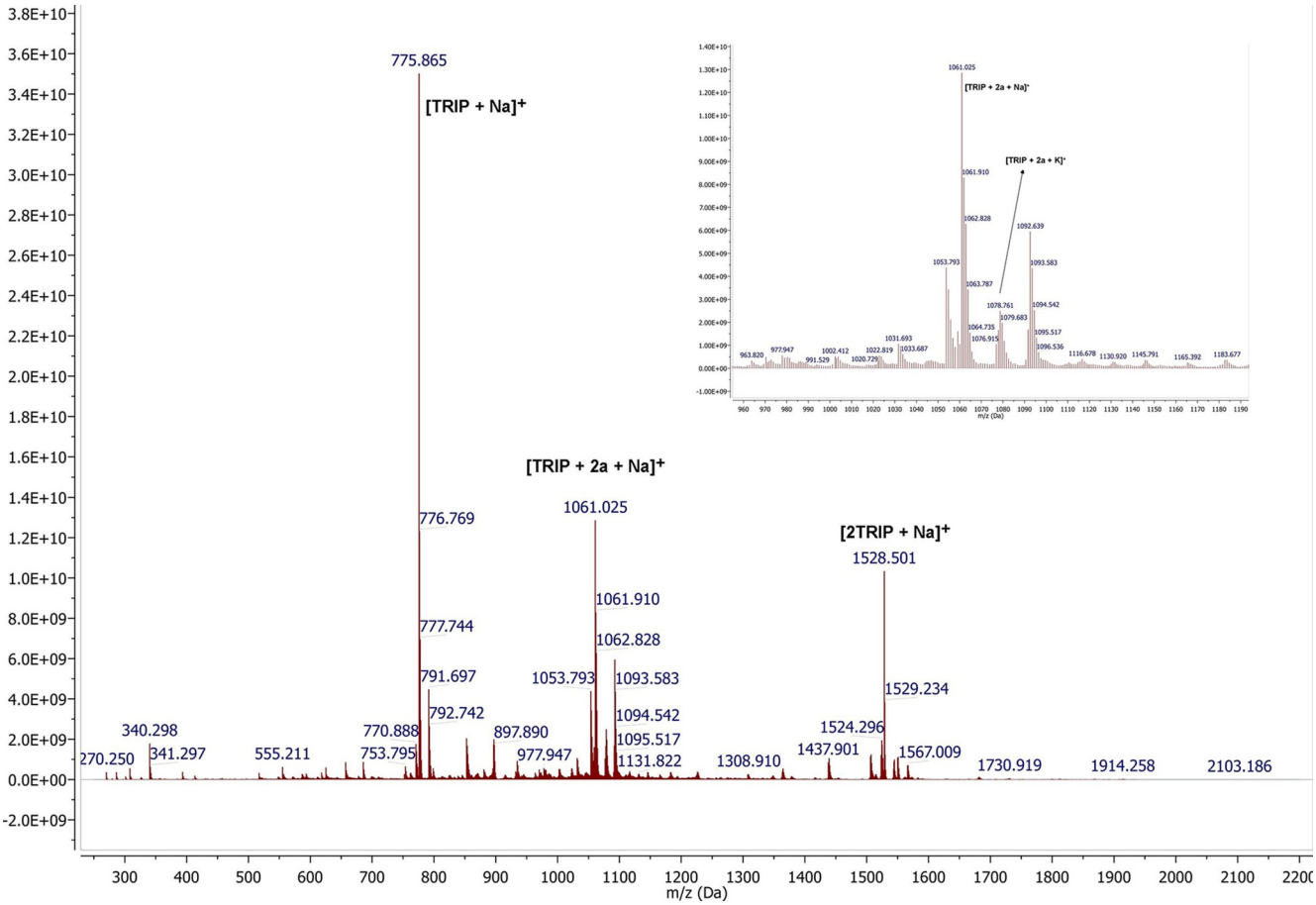

Figure 8. Positive ion ESI-MS spectrum of a mixture of the TRIP and allenamide **2a** from ion trapping. The MS spectrum shows the presence of [TRIP + **2a** + Na^+] ($m/z = 1061.025$) and [TRIP + **2a** + K^+] ($m/z = 1078.761$).

chiral phosphoric acid (Brønsted acid). The structure of the catalyst allows the formation of an initial molecular aggregate **I1** where indole and allenamide simultaneously interact with the phosphoric acids through hydrogen contacts. The role of the catalyst can be compared with that of an enzyme that brings the reactants into close proximity in the right relative orientation required by the chemical process. Within this initial molecular aggregate, the chiral promoter (phosphoric acid) can form a covalent adduct by reacting with the allenamide. The indole moiety is not involved in the formation of the covalent adduct. In the course of this initial transformation, which represents the rate-determining step of the entire process, indole remains bonded to the catalyst through a rather strong hydrogen bond. The indole (nucleophile) can take on two different orientations that make the *Re* or *Si* prochiral face available to the subsequent electrophilic attack of allenamide. The attack on the indole faces results in two different reaction paths (path R and path S) and two different stereoisomeric products differing in the configuration of the new stereocenter at the C3-indole position.

The initial molecular aggregate **I1(*S*)** that originates path S is more stable than the aggregate **I1(*R*)** that generates path R. The same order of stability was found for the two species originated by the interaction of the covalent adduct with the indole fragment exposing either the *Re* face (**I2(*R*)** species) or the *Si* face (**I2(*S*)** species). Similarly, the transition state leading to **I2(*S*)** is more stable than that leading to **I2(*R*)**. This is due to the more favorable non-covalent interactions (hydrogen bonds) that favor the structural arrangement where the *Si* face is available for the nucleophilic attack on allenamide.

Our computations demonstrated that the first step (**I1**→**I2**), which is rate-determining, is also the enantio-discriminating step of the process and the greater stability of path S explains the high stereoselection experimentally observed (*ee* = 92%) for the product with configuration *S* at C3. As the activation energy for the two transformations **I1(*S*)**→**I2(*S*)** and **I1(*R*)**→**I2(*R*)** are approximately the same, it is the equilibrium distribution of the two initial molecular aggregates **I1(*S*)** and **I1(*R*)**, which determines the final product ratio. This means, in turn, that the enantioselectivity of the process is due to the more stabilizing non-bonded interactions favoring the arrangement **I1(*S*)** where indole makes the *Si* face available for the nucleophilic attack.

Thus, the hypothesis for the initial formation of a 1:1 covalent adduct represents the real (unusual) activation mode of the present chiral proton-based catalysis. As it is central in our mechanistic hypothesis, we proved experimentally its existence by ionic trap mass spectroscopy. In the second phase of the process, the formation of the covalent adduct delivers a chiral α-amino allylic phosphate, which undergoes dearomative condensation with indoles through an enantioselective S_N2'-type mechanism.

Experimental Section

General methods

The MS and MS/MS analyses were performed with an Agilent Technologies-Bruker MSD Ion Trap 1100 Series with an electrospray (ESI) interface; the injections were performed with syringe infusion pump KD Scientific and 1.0 mL Hamilton syringe. The ESI source settings were: ion-spray voltage 4500 V in positive mode and 3500 V in negative mode; drying gas temperature 350 °C; nebulizing gas pressure 7.0 psi (nitrogen); drying gas flow 13.0 L min^{-1}. Multiple reaction monitoring (MRM) was optimizing by using helium as the collision gas.

Computational details

All DFT computations were carried out by using the Gaussian 09 series of programs.[18] The M06-2X functional proposed by Truhlar and Zhao was used.[19] According to a locally dense basis set (LDBS) approach, the model system was partitioned into different regions, which were assigned basis sets of different accuracy. One region included the molecules directly involved in the reaction (indole and allenamide) and the atoms of the central substructure of the BA*-H catalyst (phosphate and BINOL moiety); for this region, we used the 6-31G* basis set.[18] All remaining atoms, forming the other region, were described by the 3–21G* basis set.[18] The geometries of the various critical points on the potential surface were fully optimized with the gradient method available in Gaussian 09, in the presence of solvent effects (polarizable continuum model (PCM) calculations)[20] to simulate the experimental conditions (solvent emulated was benzene, $\varepsilon = 2.27$). Furthermore, harmonic vibrational frequencies were computed for all critical points. To obtain a better estimate of the reaction energetics, we carried out single point PCM calculations with the 6–31 + G* basis set on all atoms.[18]

Acknowledgments

The University of Bologna is kindly acknowledged for financial support. M.B. also thanks Cost Action 1407. G. P. Miscione also would like to acknowledge the High-Performance Computing center of the Universidad de los Andes, Bogotá (Colombia) for support and computational resources and the FAPA project of Sciences Faculty of Universidad de los Andes, Bogotá (Colombia).

Conflict of interest

The authors declare no conflict of interest.

Keywords: allenamide indoles · asymmetric catalysis · covalent catalysis · dearomatization · DFT computations · reaction mechanism

[1] For a selection of review articles on asymmetric BINOL-based chiral phosphoric acid catalysis, see: a) T. Akiyama, *Chem. Rev.* **2007**, *107*, 5744 – 5758; b) M. Terada, *Chem. Commun.* **2008**, 4097 – 4112; c) D. Parmar, E. Sugiono, S. Raja, M. Rueping, *Chem. Rev.* **2014**, *114*, 9047 – 9153; d) *Asymmetric Brønsted Acid Catalysis* (Eds.: M. Rueping, D. Parmar, E. Sugiono), Wiley-VCH, Weinheim, **2016**.

[2] M. R. Monaco, G. Pupo, B. List, *Synlett* **2016**, *27*, 1027 – 1040.

[3] a) R. J. Phipps, G. L. Hamilton, F. D. Toste, *Nat. Chem.* **2012**, *4*, 603 – 614; b) M. Mahlau, B. List, *Angew. Chem. Int. Ed.* **2013**, *52*, 518 – 533; *Angew. Chem.* **2013**, *125*, 540 – 556; c) K. Brak, E. N. Jacobsen, *Angew. Chem. Int. Ed.* **2013**, *52*, 534 – 561; *Angew. Chem.* **2013**, *125*, 558 – 588.

[4] a) N. D. Shapiro, V. Rauniyar, G. L. Hamilton, J. Wu, F. D. Toste, *Nature* **2011**, *470*, 245 – 250; b) Z. Sun, G. A. Winschel, P. M. Zimmerman, P. Nagorny, *Angew. Chem. Int. Ed.* **2014**, *53*, 11194 – 11198; *Angew. Chem.* **2014**, *126*, 11376 – 11380; see also L. Ackermann, A. Althammer, *Synlett* **2008**, 995 – 998.

[5] a) M. Bandini, A. Eichholzer, *Angew. Chem. Int. Ed.* **2009**, *48*, 9533 – 9537; *Angew. Chem.* **2009**, *121*, 9697 – 9701; b) M. Bandini, A. Gualandi, M. Monari, A. Romaniello, D. Savoia, M. Tragni, *J. Organomet. Chem.* **2011**, *696*, 338 – 347; c) G. Cera, P. Crispino, M. Monari, M. Bandini, *Chem. Commun.* **2011**, *47*, 7803 – 7805; d) G. Cera, S. Piscitelli, M. Chiarucci, G. Fabrizi, A. Goggiamani, R. S. Ramån, S. P. Nolan, M. Bandini, *Angew. Chem. Int. Ed.* **2012**, *51*, 9891 – 9895; *Angew. Chem.* **2012**, *124*, 10029 – 10033; e) G. Cera, M. Chiarucci, A. Mazzanti, M. Mancinelli, M. Bandini, *Org. Lett.* **2012**, *14*, 1350 – 1353; f) M. Chiarucci, E. Matteucci, G. Cera, G. Fabrizi, M. Bandini, *Chem. Asian J.* **2013**, *8*, 1776 – 1779; g) M. Chiarucci, R. Mocci, L.-D. Syntrivanis, G. Cera, A. Mazzanti, M. Bandini, *Angew. Chem. Int. Ed.* **2013**, *52*, 10850 – 10853; *Angew. Chem.* **2013**, *125*, 11050 – 11053; h) M. Jia, M. Monari, Q.-Q. Yang, M. Bandini, *Chem. Commun.* **2015**, *51*, 2320 – 2323; i) P. Giacinto, G. Cera, A. Bottoni, M. Bandini, G. P. Miscione, *ChemCatChem* **2015**, *7*, 2480 – 2484; j) Q.-Q. Yang, M. Marchini, W.-J. Xiao, P. Ceroni, M. Bandini, *Chem. Eur. J.* **2015**, *21*, 18052 – 18056; k) E. Manoni, A. De Nisi, M. Bandini, *Pure Appl. Chem.* **2016**, *88*, 207 – 214; l) A. De Nisi, S. Sierra, M. Ferrara, M. Monani, M. Bandini, *Org. Chem. Front.* **2017**, *4*, 1849 – 1853.

[6] a) L.-L. Wei, H. Xiong, R. P. Hsung, *Acc. Chem. Res.* **2003**, *36*, 773 – 782; b) T. Lu, Z. Lu, Z.-X. Ma, Y. Zhang, R. P. Hsung, *Chem. Rev.* **2013**, *113*, 4862 – 4904; and references therein; c) E. Manoni, M. Bandini, *Eur. J. Org. Chem.* **2016**, 3135 – 3142.

[7] a) M. Jia, G. Cera, D. Perrotta, M. Bandini, *Chem. Eur. J.* **2014**, *20*, 9875 – 9878; b) L. Rocchigiani, M. Jia, M. Bandini, A. Macchioni, *ACS Catal.* **2015**, *5*, 3911 – 3915.

[8] Z.-Q. Shen, X.-X. Li, J.-W. Shi, B.-L. Chen, Z. Chen, *Tetrahedron Lett.* **2015**, *56*, 4080 – 4083.

[9] H. G. Raubenheimer, H. Schmidbaur, *Organometallics* **2012**, *31*, 2507 – 2522.

[10] C. Romano, M. Jia, M. Monari, E. Manoni, M. Bandini, *Angew. Chem. Int. Ed.* **2014**, *53*, 13854 – 13857; *Angew. Chem.* **2014**, *126*, 14074 – 14077.

[11] H. Wu, Y.-P. He, F. Shi, *Synthesis* **2015**, *47*, 1990 – 2016.

[12] a) V. Rauniyar, A. D. Lackner, G. L. Hamilton, F. D. Toste, *Science* **2011**, *334*, 1681 – 1684; b) S. Harada, S. Kuwano, Y. Yamaoka, K. Yamada, K. Takasu, *Angew. Chem. Int. Ed.* **2013**, *52*, 10227 – 10230; *Angew. Chem.* **2013**, *125*, 10417 – 10420; c) W.-W. Zi, Y.-M. Wang, F. D. Toste, *J. Am. Chem. Soc.* **2014**, *136*, 12864 – 12867.

[13] For seminal works in the field, see: a) J. W. Yang, M. T. Hechavarria Fonseca, N. Vignola, B. List, *Angew. Chem. Int. Ed.* **2005**, *44*, 108 – 110; *Angew. Chem.* **2005**, *117*, 110 – 112; b) S. G. Ouellet, J. B. Tuttle, D. W. C. MacMillan, *J. Am. Chem. Soc.* **2005**, *127*, 32 – 33; c) M. Rueping, E. Sugiono, C. Azap, T. Theissmann, M. Bolte, *Org. Lett.* **2005**, *7*, 3781 – 3783.

[14] a) M. Terada, K. Sorimachi, *J. Am. Chem. Soc.* **2007**, *129*, 292 – 293; b) Y.-X. Jia, J. Zhong, S.-F. Zhu, C.-M. Zhang, Q.-L. Zhou, *Angew. Chem. Int. Ed.* **2007**, *46*, 5565 – 5567; *Angew. Chem.* **2007**, *119*, 5661 – 5663; c) M. Terada, K. Moriya, K. Kanomata, K. Sorimachi, *Angew. Chem. Int. Ed.* **2011**, *50*, 12586 – 12590; *Angew. Chem.* **2011**, *123*, 12794 – 12798.

[15] For general highlights/reviews on allylations of indoles, see: a) M. Bandini, *Angew. Chem. Int. Ed.* **2011**, *50*, 994 – 995; *Angew. Chem.* **2011**, *123*, 1026 – 1027; b) M. Bandini, G. Cera, M. Chiarucci, *Synthesis* **2012**, 504 – 512; c) A. Quintavalla, M. Bandini, *ChemCatChem* **2016**, *8*, 1437 – 1453.

[16] For comprehensive surveys on asymmetric dearomatization processes, see: a) A. R. Pape, K. P. Kaliappan, E. P. Kündig, *Chem. Rev.* **2000**, *100*, 2917 – 2940; b) S. P. Roche, J. A. Porco, Jr., *Angew. Chem. Int. Ed.* **2011**, *50*, 4068 – 4093; *Angew. Chem.* **2011**, *123*, 4154 – 4179; c) C.-X. Zhuo, W. Zhang, S.-L. You, *Angew. Chem. Int. Ed.* **2012**, *51*, 12662 – 12686; *Angew. Chem.* **2012**, *124*, 12834 – 12858; d) C. C. J. Loh, D. Enders, *Angew. Chem. Int. Ed.* **2012**, *51*, 46 – 48; *Angew. Chem.* **2012**, *124*, 46 – 49; e) C.-Z. Zhuo, C. Zheng, S.-L. You, *Acc. Chem. Res.* **2014**, *47*, 2558 – 2573; f) C. Zheng, S.-L. You, *Chem* **2016**, *1*, 830 – 857; g) *Asymmetric Dearomatization Reactions* (Ed.: S.-L. You), Wiley-VCH, Weinheim, **2016**; h) W.-T. Wu, L. Zhang, S.-L. You, *Chem. Soc. Rev.* **2016**, *45*, 1570 – 1580; i) X.-W. Liang, C. Zheng, S.-L. You, *Chem. Eur. J.* **2016**, *22*, 11918 – 11933; j) S. Park, S. Chang, *Angew. Chem. Int. Ed.* **2017**, *56*, 7720 – 7738; *Angew. Chem.* **2017**, *129*, 7828 – 7847.

[17] A. Bottoni, C. Z. Lanza, G. P. Miscione, D. Spinelli, *J. Am. Chem. Soc.* **2004**, *126*, 1542 – 1550.

[18] Gaussian 09, revision B.01, M. J. Frisch, G. W. Trucks, H. B. Schlegel, G. E. Scuseria, M. A. Robb, J. R. Cheeseman, G. Scalmani, V. Barone, B. Mennucci, G. A. Petersson, H. Nakatsuji, M. Caricato, X. Li, H. P. Hratchian, A. F. Izmaylov, J. Bloino, G. Zheng, J. L. Sonnenberg, M. Hada, M. Ehara, K. Toyota, R. Fukuda, J. Hasegawa, M. Ishida, T. Nakajima, Y. Honda, O. Kitao, H. Nakai, T. Vreven, J. A. Montgomery, Jr., J. E.; Peralta, F. Ogliaro, M. Bearpark, J. J. Heyd, E. Brothers, K. N. Kudin, V. N. Staroverov, R. Kobayashi, J. Normand, K. Raghavachari, A. Rendell, J. C. Burant, S. S. Iyengar, J. Tomasi, M. Cossi, N. Rega, J. M. Millam, M. Klene, J. E. Knox, J. B. Cross, V. Bakken, C. Adamo, J. Jaramillo, R. Gomperts, R. E. Stratmann, O. Yazyev, A. J. Austin, R. Cammi, C. Pomelli, J. W. Ochterski, R. Martin, K. Morokuma, V. G. Zakrzewski, G. A. Voth, P. Salvador, J. J. Dannenberg, S. Dapprich, A. D. Daniels, J. B. Foresman, J. V. Ortiz, J. Cioslowski, D. J. Fox, Gaussian, Inc., Wallingford CT, **2009**.

[19] a) Y. Zhao, D. G. Truhlar, *J. Phys. Chem. A* **2004**, *108*, 6908 – 6918; b) Y. Zhao, D. G. Truhlar, *J. Phys. Chem. A* **2005**, *109*, 5656 – 5667; c) Y. Zhao, D. G. Truhlar, *J. Phys. Chem. B* **2005**, *109*, 19046 – 19051; d) Y. Zhao, D. G. Truhlar, *Acc. Chem. Res.* **2008**, *41*, 157 – 167.

[20] J. Tomasi, B. Mennucci, R. Cammi, *Chem. Rev.* **2005**, *105*, 2999 – 3094.